Vol. 18, No. 1 (2019) 339-347
Revista Mexicana de Ingeniería Química

ISOMORPHIC SUBSTITUTION OF Mg^{2+} BY Al^{3+} ON MgO: EFFECTS ON BASICITY, TEXTURAL PROPERTIES AND MICROSTRUCTURE

SUSTITUCIÓN ISOMÓRFICA DE Mg^{2+} POR Al^{3+} EN MgO: EFECTOS EN LA BASICIDAD, PROPIEDADES TEXTURALES Y MICROESTRUCTURA

L. Pérez-Cabrera, J.N. Díaz de León*, J. Antúnez-García, D.H. Galván, G. Alonso-Núñez, S. Fuentes-Moyado
Universidad Nacional Autónoma de México, Centro de Nanociencias y Nanotecnología. Km. 107 Carretera Tijuana-Ensenada, Ensenada, B. C. México.
Received: June 21, 2018; Accepted: July 18, 2018

Abstract
The influence of aluminum atoms on the surface and structural properties of distinct mixed oxides MgAl-x (x=Al/(Al+Mg)= 0, 0.20, 0.25, 0.33 and 1.0) was studied. Hammet titration results showed that the isomorphic substitution of Mg by Al atoms induced a basicity character decrease. Theoretical DFT studies of MgAl-x oxides basicity through the oxygen Mulliken charges showed a similar trend to that observed experimentally. The effect in the textural properties as a function of the Al content was reflected directly in the surface area and pore size distributions. Noteworthy was to observed the morphological modification on the mixed oxides with the Al content, passing from nanorods in pure MgO to hexagonal platelets in the binary oxides.
Keywords: DFT studies, magnesia-alumina, acid-base oxides, isomorphic substitution, nanostructures.

Resumen
Se estudió la influencia de los átomos de Al sobre las propiedades de diferentes óxidos MgAl-x (x=0, 0.20, 0.25, 0.33 and 1.0). Los resultados de titulación con indicador de Hammet mostraron que la sustitución isomorfa de Mg por Al induce reducción de la basicidad. El estudio teórico por DFT de la basicidad a través de cargas de Mulliken en el átomo de oxígeno mostró una tendencia similar a la observada experimentalmente. El efecto en las propiedades texturales en función del contenido de Al, se observó reflejado directamente en el área superficial y las distribuciones de tamaño de poro. Interesantemente, la modificación con Al en los óxidos binarios cambio la morfología pasando de nanorodillos en MgO puro a platos hexagonales en los óxidos binarios.
Palabras clave: estudios DFT, magnesia-alúmina, óxidos ácidos-básicos, sustitución isomórfica, nanoestructuras.

1 Introduction

The $MgO\text{-}Al_2O_3$ mixed oxides have been used as humidity sensors, catalysts, photocatalysts, gas adsorbents, in anionic exchange, as a drug carrier systems, among others (Klym *et al*., 2015; Gomes *et al*., 2016; Lee *et al*., 2016; Ramos-Ramirez *et al*., 2017). The $MgO\text{-}Al_2O_3$ binary oxides usually were used as catalysts by themselves or as a supports in diverse reactions, i.e., alcohols decomposition (Corma *et al*., 1994), biodiesel synthesis (Xie *et al*., 2006; Stewart *et al*., 2015), or fossil fuels hydrotreatment (Zhao *et al*., 2003; Coelho *et al*., 2015). These binary oxides exhibit basicity due to its surface OH-groups, electron pairs from oxygen in $Mg^{2+}\text{-}O^{2-}$ and $Al^{3+}\text{-}O^{2-}$, and mainly of O^{2-} isolated anions (Di Cosimo *et al*., 1998). The catalytic performance of MgO in different reactions involves primarily the rupture of a heterolytic bond where the basic property of an O^{2-} anion prevails over the acid property of Al^{3+} or Mg^{2+} ions. The $MgO\text{-}Al_2O_3$ oxides may form a wide variety of nanostructures such as nanosheets, nanorods, nanocubes, among others. (Yan & Xue, 2005). From experimental and theoretical observations, small-MgO clusters prefer nanorod shape morphology instead to the bulk-like structure. One- or two-dimensional structures like nanorods or nanosheets are of paramount importance due to its potential applications in optical and electronic devices (Zhao *et al*., 2014), bio-inorganic sensors (Klym, Hadzaman *et al*., 2015), solid-basic catalysts (Nasibulin *et al*., 2010; Bagheri & Moradi,

* *Corresponding author. E-mail*: noejd@cnyn.unam.mx
doi: https://doi.org/10.24275/uam/izt/dcbi/revmexingquim/2019v18n1/Perez
issn-e: 2395-8472

2014), and as a supports (Zhang *et al*., 2015).

The isomorphic atomic-substitution is a well-known feature of clay materials like zeolites or hydrotalcites. In the oxide mixtures of hydrotalcites, their metallic composition determines its acid-base properties and its catalytic performance (Kraushaarczarnetzki *et al*., 1993; Corma *et al*., 2001; Sanderson *et al*., 2013; Morales-Zarate, 2018). In that sense, many experimental and density functional theoretical studies (DFT) have been successfully correlated in the case of zeolites and MgO materials (Deka *et al*., 2000; Petitjean *et al*., 2014; Begum & Deka, 2017) trying to estimate and understand its properties.

In the current work, we explore the effects of aluminum ion isomorphic substitution on the MgO-Al synthesized oxides materials. The crystalline structure, morphology, textural properties, and basicity of these materials are reported as a function of the Al/(Al+Mg) ratio. Also, the isomorphic atomic-substitution of Mg by Al will be examined through DFT calculations based on Mulliken charge analyses, and partial density of states (DOS).

2 Materials and methods

All materials were synthesized by a modified coprecipitation method (Cavani *et al*., 1991), varying the Al/(Al+Mg)=x atomic ratio with x=0, 0.20, 0.25, 0.33 and 1.0 and labeled as MgAl-x. The Al and Mg nitrates ($Al(NO_3)_3{\cdot}9H_2O$ and $Mg(NO_3)_2{\cdot}\ 6H_2O$) were used as metal oxide precursors according to the Al/(Al+Mg) atomic ratio of each intended preparation. The precipitation solution of NaOH-Na_2CO_3 (3.15 M and 2.86 M), was added to the metal precursor solution at 2 mL·min^{-1}. The pH was kept at 12, and the synthesis temperature was set it at 90 °C. The resulting solution was kept under stirring (550 rpm) for 48 h. Then the obtained gel was aged for 48 h. The obtained white powder was neutralized with deionized water and then dried at 80°C overnight. The pure MgAl-0 (MgO) was prepared similarly to the other samples without the aluminum precursor addition in the case of MgAl-1 (γ Al_2O_3) the Mg precursor was not included. All samples were calcined at 500°C for 4 h.

The chemical composition was determined by inductively coupled plasma optical emission spectroscopy (ICP-OES) using a Vista-MPX Varian with CCD detectors. The surface basicity was determined by Hammet-titration method with benzoic acid in benzene solution using bromothymol blue as an indicator (Tanabe, 1970). For the thermogravimetric (TG) analysis, the uncalcined samples (~30 mg) were analyzed by heating from 30 to 700ºC at 10ºC·min^{-1} in the airflow of 10 mL·min^{-1} in a TA Instruments SDT-Q600 (1S). X-ray diffraction (XRD) was done using a Philips X'pert diffractometer (2S), with CuKα radiation (1.541 Å), at 45 kV and 40 mA. The microstructural features were studied by transmission electron microscopy (TEM) using a JEOL JEM-2010 microscope with 200 kV accelerating voltage. X-ray photoelectron spectroscopy (XPS) was performed in a SPECS spectrometer with a PHOIBOS WAL analyzer, using monochromatic Al-k$_\alpha$ radiation (1486.6 eV). The textural properties were measured by N_2 physisorption in a Tristar-II 3020 Micromeritics analyzer through the BET equation for specific surface area (Sing, 2014), and the BJH method for pore size distribution approximations (Barrett *et al*., 1951).

Theoretical calculations were based on DFT method to obtain the Mulliken charges (MC) and partial density of states (PDOS) considering the Perdew-Burke-Ernzerhof (PBE) gradient-corrected functional (Perdew *et al*., 1996; Antúnez-García *et al*., 2015). Simulation started with the unit cell of bulk MgO (group Fm-3m), and it was adjusted by isomorphic substitution of Mg atoms by Al atoms to build the distinct solid solutions. Also, for comparison, the $MgAl_2O_4$ spinel type compound was calculated (3S).

3 Results and discussion

The bulk composition of calcined materials was measured by ICP and listed in Table 1. The chemical analysis confirmed that samples were successfully prepared with the nominal ratios intended with no more of 10% deviation.

The textural properties are given in Table 1. The MgAl-0 and MgAl-1 materials exhibited areas higher than 200 $m^2{\cdot}\ g^{-1}$. However, the MgAl-x binary oxides displayed smaller surface areas c.a. 120 $m^2{\cdot}\ g^{-1}$. The pore volume decreased as follows: 0.84, 0.51 and 0.24 $cm^3{\cdot}\ g^{-1}$ for MgAl-0.20, MgAl-0.25 and MgAl-0.33 respectively. The N_2 adsorption-desorption isotherms for the samples are presented in Fig. 1. For MgAl-0 and MgAl-1 samples, the isotherms resulted in type IV with hysteresis cycles type H2 and H4, respectively (see Fig. 1a).

Table 1: ICP Composition, textural properties, basicity and XPS quantification for the MgAl-x materials.

MgAl-x	ICP		x^b	S_{BET}	P_s	P_v	Basicity[d]	XPS		x^c
$x^a_{nominal}$	% Al	%Mg	ICP	($m^2 \cdot g^{-1}$)	(nm)	($cm^3 \cdot g^{-1}$)	(mmol·g^{-1})	% Al	%Mg	XPS
0.00	0.0	26.6	0.00	200	17.0	1.14	0.30	-	21.1	0.0
0.20	4.6	16.5	0.22	133	22.3	0.84	0.17	4.4	11.1	0.28
0.25	6.3	17.9	0.26	127	12.8	0.51	0.23	4.8	10.9	0.30
0.33	9.4	17.6	0.35	119	17.9	0.24	0.17	6.3	9.3	0.4
1.00	30.8	0.0	1.00	262	5.4	0.46	0.12	25.6	-	1.0

[a,b,c]x = Al/(Al+Mg) nominal and surface compositions, [d]Titration with benzoic acid.

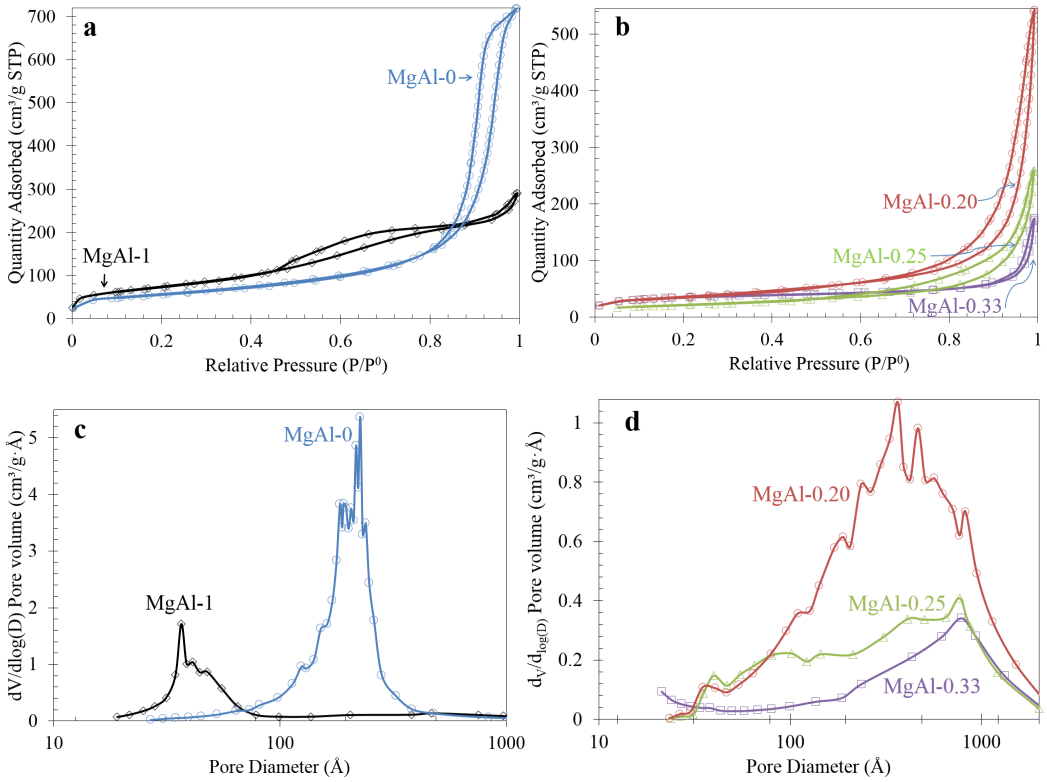

Figure 1. N_2 adsorption-desorption isotherms of pure a) MgAl-0 and MgAl-1, and b) mixed materials. Average pore size distribution of c) MgAl-0 and MgAl-1, and d) mixed oxides.

The hysteresis for MgAl-0 means a distribution of small mesopores (2-5 nm), generally associated with ink-bottle pores. The hysteresis type H4 was observed for MgAl-1, this kind of hysteresis loop is associated with microporosity, which is reflected in the appearance of a horizontal plateau at low relative-pressures (P/P°). In the case of the binary mixed oxides, the isotherms revealed to be type II (Fig. 1b) and H3 type hysteresis loop. This kind of loop revealed a non-uniform porosity of slit-shaped pores.

Fig. 1c shows the pore size distributions for MgAl-0 presenting mainly mesoporous pore-size distribution near to 17 nm. Otherwise, the MgAl-1 presents two peaks centered at 3.8 and 4.7 nm. Similarly, to the pore size distribution for MgAl-1, binary oxides displayed the presence of pores with a diameter close to 3.8 nm, and with a sharp pore-size distribution. Binary oxides present mesopores and macropores (Fig. 1d), the MgAl-0.20 sample present smaller pores and a narrower pore size distribution than the other two materials. The MgAl-0.25 sample presents a broad range of pore sizes. The MgAl-0.33 solid exhibits a pore-size distribution mainly in the macroporous region with a maximum of ~78.5 nm.

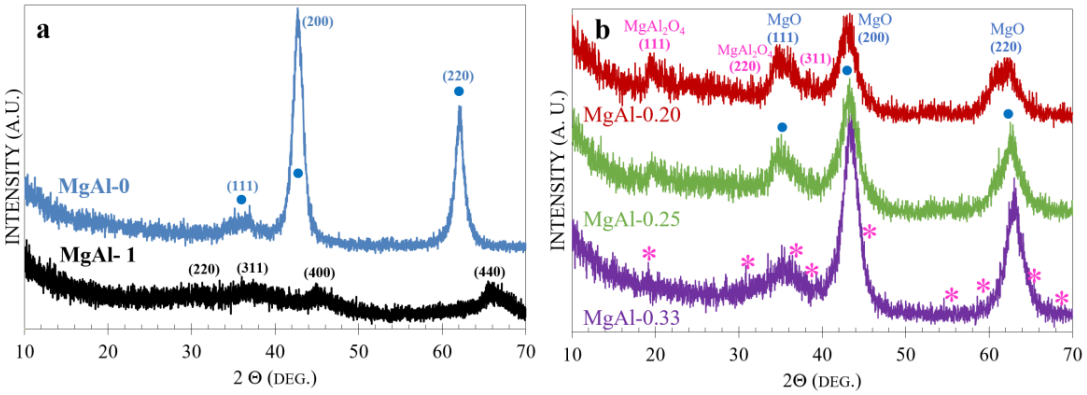

Figure 2. XRD patterns of materials calcined at 500 °C a) MgAl-0 and MgAl-1, b) mixed oxides. The MgO and $MgAl_2O_4$ structures are indicated in the figure with a blue circle or with a pink star, respectively.

This effect could be related with the synthesis procedure, specifically to the calcination process in which the wall structure can collapse. Our TG experiments provided in the supplementary information (1S) suggested that when the Al/(Al+Mg) ratio increases the mass loss increases as well. Therefore the water molecules, interlayer carbonates (CO_3^{2-}) and nitrates (NO_3^-) that stabilize the global structure where removed almost 20% more in the MgAl-0.33 in comparison to the MgAl-0.20 and MgAl-0.25 samples. Also, the XRD results of the uncalcined samples (2S) revealed that the formation of the hydrotalcite structure with JCPDS No. 00-022-0700 decrease with the increase in the Al/(Al+Mg) ratio.

Hence, the isomorphic substitution of Mg by Al decreases, inducing the formation of an amorphous bulk material with the observed decrease in the textural properties.

The diffraction patterns of calcined materials are shown in Fig. 2. The mixed MgAl-x samples obtained at the calcination temperatures of 500 °C present diffraction peaks at 42.74°, 42.95°, 43.19°, and 43.38° with FWHM of 1.46, 2.25, 2.17 and 2.13, respectively (Gaussian fitting of the highest peak). The obtained average crystallite size by the Scherer's formula was 6.10, 3.97, 4.12 and 4.20 nm for MgAl-0, MgAl-0.20, MgAl-0.25, and MgAl-0.33 materials respectively. The mixed oxides also presented structural changes as the aluminum concentration increases. The (200) plane of MgO periclase phase was shifted from 42.7° to 43.9° probably due to the cation size difference (Mg^{2+}=0.65 Å, Al^{3+} = 0.50 Å). This is in good agreement with a previous report where it was showed that progressive isomorphic replacement of Mg by Al decreases the MgO crystallographic cell (Corma, Fornes *et al*., 1994). In the case of single oxides, the diffraction pattern for MgAl 1 (Fig. 2a) is characteristic of γ-Al_2O_3 with typical diffraction lines at 2θ = 32º, 39º, 46º and 67º corresponding to the JCPDS No. 47-1308 card. The MgAl-0 and the mixed oxides present a cubic type structure associated with MgO periclase (JCPDS No. 45-0946) with reflections at 2θ = 36.5, 42.9º, 62.7º.

The basicity was determined experimentally by Hammett-titration method and theoretically through oxygen Mulliken-atomic charges analysis. The basic-strength results obtained by the Hammet-titration method are shown in Table 1. The observed trend resulted as follows: MgAl-0 >MgAl-0.25 >MgAl-0.33 ~MgAl-0.20 >MgAl-1. The binary oxides basicity decreased with aluminum content reaching a maximum at x=0.25. The low basicity of MgAl-0.20 may be explained either as a moderate dispersion of Al^{3+} ions in MgO or by the formation of segregated $MgAl_2O_4$ spinels type structures (Di Cosimo, Díez *et al*., 1998). The further decrease observed for the MgAl-0.33 material corresponds well with the instability of the material due to a defective structure with high aluminum content (Fishel & Davis, 1994). Our results agreed with reports showing that the function of aluminum in binary oxides is to decrease the basic properties forming medium basic-sites (H≥7.1) (Navajas *et al*., 2010). The MgAl 1 basicity value agreed with that early reported by Tanabe (Tanabe, 1970).

According to Deka *et al*. (2000), the oxygen atoms with partial negative charge behave as basic sites. Therefore, the analysis of the Mulliken Charges (MC) for the

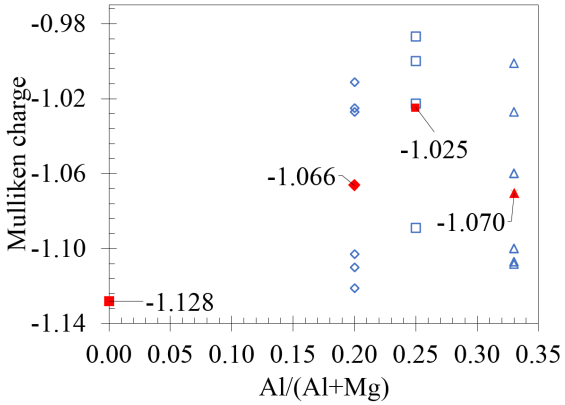

Figure 3. MC for oxygen atoms as function of atomic ratio x for MgAl-x mixed oxides. Average MC values are indicated by red symbols.

O atoms in the materials can be used to determine the basic strength. General trends of MC for all atoms involved in the materials were calculated, although only the values obtained for oxygen atoms charges are presented in Fig. 3. This Figure shows that all oxygen atoms in magnesia (MgAl-0) presents the same MC values. However, for these mixed oxides, the O atoms charge presents a dispersive behavior as a function of the Al/(Al+Mg) ratio. For these oxides, it should be noted that, at x=0.25, the average lowest negative charge occupation occurs. This implies that the oxygen atoms become more reactive due to the charge deficiency at the valence shell. Then, the observed trend basicity for this case is MgAl-0.0 (-1.128) >MgAl-0.33(-1.070) ~MgAl-0.20 (-1.066) >MgAl-0.66 (-1.056) >MgAl-0.25 (-1.025) >MgAl 1.0 (-0.376). A similar MC trend was observed for Al and Mg atoms (see 3S).

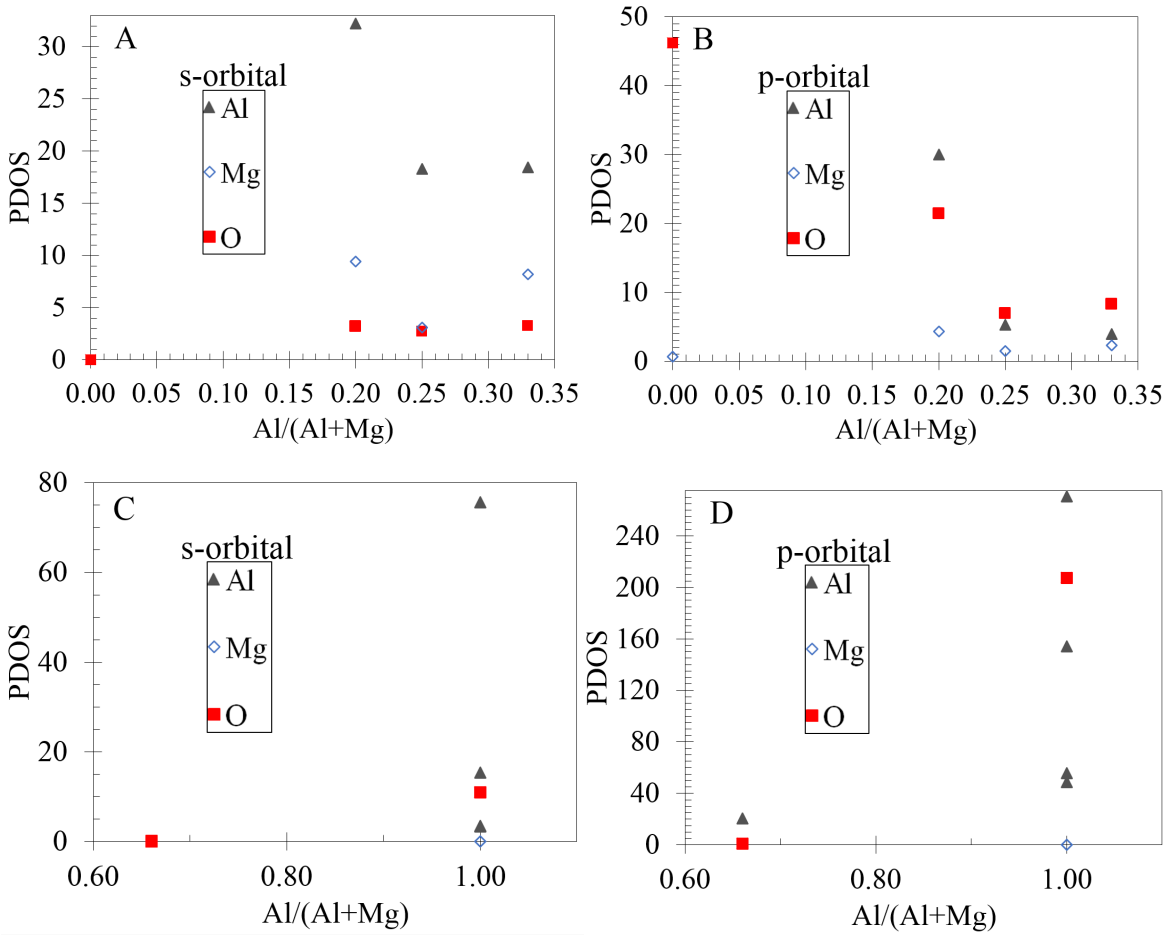

Figure 4. s and p-orbitals contributions (PDOS) at the Fermi level for: distinct MgAl-x mixed oxides (A and B) and $MgAl_2O_4$ spinel and pure γ-Al_2O_3 (C and D). Labels for distinct atomic species are described in each Figure.

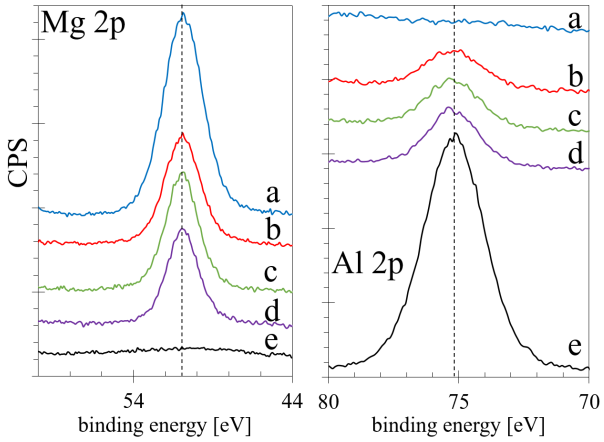

Figure 5. XPS analysis of Mg 2p and Al 2p orbitals for a) 0, b) 0.20, c) 0.25, d) 0.33 and e) 1 for the MgAl-x materials.

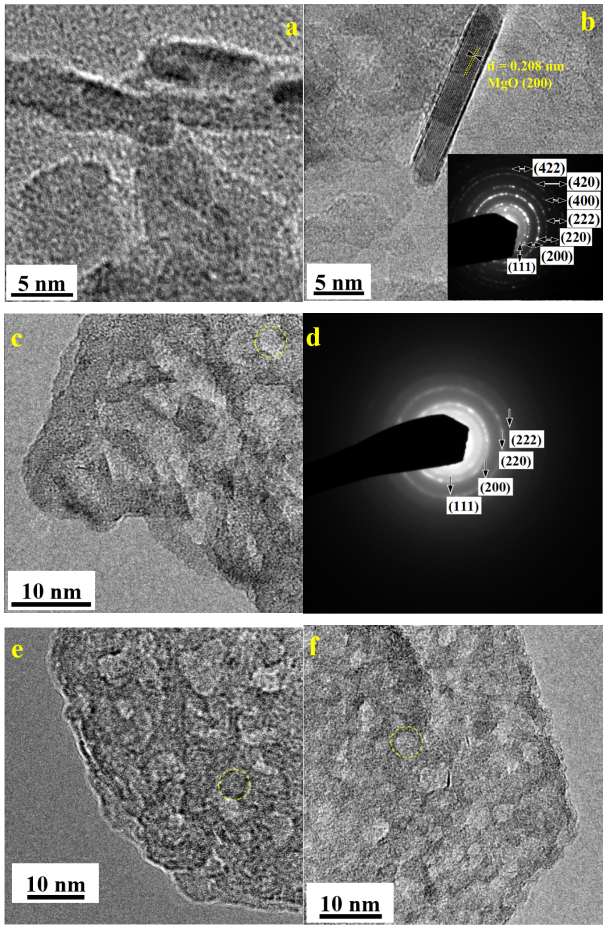

Figure 6. Micrographs showing a) small MgAl-0 rods and semi-hexagonal nanostructures, and b) isolated nanorod. MgAl-x mixed oxides with semi-hexagonal nanostructures at c) x=0.20, d) SAED pattern for MgAl-20 sample, e) x=0.25, and f) x=0.33.

Fig. 4 A-D displays the partial density of states (PDOS) contributions at the Femi level for s and p orbitals corresponding to Mg, Al, and O atoms for distinct compositions. The Figs. 4 A-B show that for pure MgO (x = 0), the oxygen atoms from the 2p orbital are responsible for electronic conduction. Contrarily in mixed oxides, oxygen atoms present s and p orbitals hybridization with considerably lower s-orbital participation. The mixed oxides also present orbitals hybridizations for Mg and Al atoms, but mainly at x = 0.25, the lowest rate of hybridization is reached for all Al, Mg, and O atoms.

It should also be noted that at this x-value the Mg PDOS orbitals participation is the lowest in the mixed oxides, according to the basicity trends above discussed. As a result, there is a promotion of Al, the inhibition of Mg participation at the Fermi level and the hybridization of s and p orbitals (for Al and O atoms) in mixed oxides. For spinel and γ-Al_2O_3 (Fig. 4 C and D) the following was observed: a) both compounds present preferential participation of Al atoms and b) mainly γ-Al_2O_3 presents p and s orbitals hybridization of both Al and O atoms.

The difference in the basicity trend observed experimentally through the Hammet-titration method (Table 1) versus the theoretical trend described by MC, could be attributed to differences on the surface chemical composition. To get insight into this matter, the surface composition for MgAl-x samples was analyzed by XPS. The XPS spectra for all samples in the core emission region of Mg 2p and Al 2p are presented in Fig. 5 and the results are listed in Table 1. The Al/(Al+Mg) experimental ratios were 0.40, 0.30 and 0.28 corresponding to MgAl-0.33, MgAl-0.25, and MgAl-0.20 respectively. Those values indicated surface aluminum enrichment, which is consistent with the formation of $MgAl_2O_4$ spinel-type structures (Cantrell *et al*., 2005; Díaz de León, 2016). The MgAl-0.20 and MgAl-0.33 oxides presented a higher Al surface enrichment than the MgAl-0.25 sample that is in agreement with the basic sites measurements.

Fig. 6a displays representative micrographs for MgAl-0 material showing MgO with semi-hexagonal nanoplates and nanorods morphologies with diameters of 3.3 to 7.1±0.1 nm and lengths up to ~71±1 nm. The micrograph in Fig. 6b shows clear nanorods lattice-fringes with an interplanar spacing (ds) of 0.208 nm corresponding to (200) plane. The electron diffraction (SAED) pattern in Fig. 6b confirmed the nanorods crystalline structure with (111), (200), (220), (222), (400), (420) and (422) planes diffractions. Micrographs for MgAl-0.20, MgAl-0.25, and MgAl-0.33 binary oxides were very similar to each other (Figs. 6c-f). On these samples, MgAl-nanoplates with wormhole-like mesoporosity arrangement (Harshad R. Patil, 2016) were observed (4S-a). Those structures presented hexagonal shape in the range of 5 nm and are associated with the hydrotalcite precursor (Hickey *et al*., 2000; Zhao, Zhang *et al*., 2014; Zarazúa-Aguilar, 2018). The SAED pattern of mixed oxides showed only (111), (200), (220), and (222) planes (Fig. 6d). The MgAl-1 material (4Sc-d) presents a sheet type structure with folds. The inset SAED-pattern for this sample showed diffraction corresponding to (311), (400), and (440) planes of γ-Al_2O_3.

Conclusions

The present study showed that the isomorphic substitution of Mg^{2+} by Al^{3+} cations in the MgO nanostructure, induce a modification in the general characteristics of the materials, i.e. textural, structural and basicity properties. Theoretical DFT-based studies showed that this substitution promotes the Al atoms participation at the Fermi level and decreases that of Mg atoms. This effect allowed the s and p orbitals hybridization (for Al and O atoms) in these binary mixed oxides. These DFT studies showed that for the mixed oxides MgAl-x the optimal Al concentration resulted in x = 0.25, consistently with the experimental results. On the other hand, the XPS data indicated an aluminum enrichment on the surface of binary oxides that induced a reduction on its basicity properties. Textural and TGA analysis of binary oxides confirmed that high aluminum concentration modified the pore size from mesoporosity to macroporosity. The TEM analysis also exhibited a change in morphology from rod-shape to plate-shape nanostructures as a function of Al addition.

Acknowledgements

We acknowledge F. Ruiz, E. Aparicio, D. Dominguez. Also to CONACyT for the scholarship 353121 of L. Pérez-Cabrera and to project SENER-CONACyT-117373 for financial support and to Super Cómputo LANCAD-UNAM-DGTIC-041 for the facilities provided.

References

Antúnez-García, J., Galván, D.H., Petranovskii, V., Posada-Amarillas, A. (2015). A DFT study of copper-oxide clusters embedded in dry and water-immersed siliceous mordenite. *Computational Materials Science 106*, 140-148.

Bagheri, Z., Moradi, M. (2014). DFT study on the adsorption and dissociation of hydrogen sulfide on MgO nanotube. *Structural Chemistry 25*, 495-501.

Barrett, E.P., Joyner, L.G., Halenda, P.P. (1951). The determination of pore volume and area distributions in porous substances. I. Computations from nitrogen isotherms. *Journal of the American Chemical Society 73*, 373-380.

Begum, P., Deka, R.C. (2017). Effect of charge on the catalytic activity of CO oxidation by zeolite supported single site palladium: A density functional study. *ChemistrySelect 2*, 8847-8855.

Cantrell, D.G., Gillie, L.J., Lee, A.F., Wilson, K. (2005). Structure-reactivity correlations in MgAl hydrotalcite catalysts for biodiesel synthesis. *Applied Catalysis A: General 287*, 183-190.

Cavani, F., Trifirò, F., Vaccari, A. (1991). Hydrotalcite-type anionic clays: Preparation, properties and applications. *Catalysis Today 11*, 173-301.

Coelho, T.L., Licea, Y.E., Palacio, L.A., Faro, A.C. (2015). Heptamolybdate-intercalated CoMgAl hydrotalcites as precursors for HDS-selective hydrotreating catalysts. *Catalysis Today 250*, 38-46.

Corma, A., Fornes, V., Rey, F. (1994). Hydrotalcites as base catalysts: Influence of the chemical composition and synthesis conditions on the dehydrogenation of isopropanol. *Journal of Catalysis 148*, 205-212.

Corma, A., Navarro, M.T., Rey, F., Rius, J., Valencia, S. (2001). Pure polymorph C of zeolite beta synthesized by using framework isomorphous substitution as a structure-directing mechanism. *Angewandte Chemie 113*, 2337-2340.

Deka, R.C., Kinkar Roy, R., Hirao, K. (2000). Basicity of the framework oxygen atom of alkali and alkaline earth-exchanged zeolites: A hard-soft acid-base approach. *Chemical Physics Letters 332*, 576-582.

Di Cosimo, J.I., Díez, V.K., Xu, M., Iglesia, E., Apesteguía, C.R. (1998). Structure and surface and catalytic properties of Mg-Al basic oxides. *Journal of Catalysis 178*, 499-510.

Díaz de León, J.N. (2016). Binary γ-Al_2O_3-α-Ga_2O_3 as supports of NiW catalysts for hydrocarbon sulfur removal. *Applied Catalysis B: Environmental 181*, 524-533.

Fishel, C.T., Davis, R.J. (1994). Characterization of magnesium-aluminum mixed oxides by temperature-programmed reaction of 2-propanol. *Langmuir 10*, 159-165.

Gomes, A., Cocke, D., Tran, D. y Baksi, A. (2016) Layered double hydroxides in energy research: Advantages and challenges. En: *Energy Technology 2015: Carbon Dioxide Management and Ather Technologies*, (A. Jha, C. Wang, N.R. Neelameggham, D.P. Guillen, L. Li, C.K. Belt, R. Kirchain, J.S. Spangenberger, F. Johnson, A.J. Gomes, A. Pandey, P. Hosemann eds.), Pp. 309-316. Springer International Publishing, Cham.

Harshad R. Patil, Z.V.P.M. (2016). Vanadium-doped magnesium oxide nanoparticles formation in presence of ionic liquids and their use in photocatalytic degradation of methylene blue. *Acta Metallurgica Sinica(English Letters) 29*, 253-264.

Hickey, L., Kloprogge, J.T., Frost, R.L. (2000). The effects of various hydrothermal treatments on magnesium-aluminium hydrotalcites. *Journal of Materials Science 35*, 4347-4355.

Klym, H., Hadzaman, I., Shpotyuk, O. (2015). Influence of sintering temperature on pore structure and electrical properties of technologically modified MgO-Al_2O_3 ceramics. *Materials Science 21*, 92-95.

Kraushaarczarnetzki, B., Dogterom, R.J., Stork, W.H.J., Emeis, K.A., Houckgeest, J.P.V. (1993). Isomorphous substitution and the generation of catalytic activity in VPI-5. *Journal of Catalysis 141*, 140-147.

Lee, J.-Y., Gwak, G.-H., Kim, H.-M., Kim, T.-i., Lee, G.J., Oh, J.-M. (2016). Synthesis of hydrotalcite type layered double hydroxide with various Mg/Al ratio and surface charge under controlled reaction condition. *Applied Clay Science 134*, 44-49.

Morales-Zarate, J., Paredes-Carrera, S., Castro-Sotelo, L. (2018). Mixed oxides of Zn/Al, Zn/Al-La and Zn-Mg/Al: Preparation, characterization and photocatalytic activity in diclofenac degradation. *Revista Mexicana de Ingeniería Química 17*, 941-953.

Nasibulin, A.G., Sun, L., Hämäläinen, S., Shandakov, S.D., Banhart, F., Kauppinen, E.I. (2010). *In situ* TEM observation of MgO nanorod growth. *Crystal Growth & Design 10*, 414-417.

Navajas, A., Campo, I., Arzamendi, G., Hernández, W.Y., Bobadilla, L.F., Centeno, M.A., Odriozola, J.A. y Gandía, L.M. (2010). Synthesis of biodiesel from the methanolysis of sunflower oil using pural® Mg-Al hydrotalcites as catalyst precursors. *Applied Catalysis B: Environmental 100*, 299-309.

Perdew, J.P., Burke, K. y Ernzerhof, M. (1996). Generalized gradient approximation made simple. *Physical Review Letters 77*, 3865-3868.

Petitjean, H., Guesmi, H., Lauron-Pernot, H., Costentin, G., Loffreda, D., Sautet, P., Delbecq, F. (2014). How surface hydroxyls enhance MgO reactivity in basic catalysis: The case of methylbutynol conversion. *ACS Catalysis 4*, 4004-4014.

Ramos-Ramirez, Esthela Gutirrez-Ortega, N.L., Tzompantzi-Morales, F., Del Angel, G.A., Martinez-Gomez, C., Pabon-Gelves, E. (2017). Effect of the Mg/Al ratio on activated sol-gel hydrotalcites for photocatalytic degradation of 2,4,6-trichlorophenol. *International Journal of Photoenergy 2017*, 1-9.

Sanderson, B.A., Sowersby, D.S., Crosby, S., Goss, M., Lewis, L.K., Beall, G.W. (2013). Charge density and particle size effects on oligonucleotide and plasmid DNA binding to nanosized hydrotalcite. *Biointerphases 8*, 1-11.

Sing, K.S.W. (2014) 7 - Assessment of surface area by gas adsorption. En: *Adsorption by Powders and Porous Solids* (second edition), Pp. 237-268. Academic Press, Oxford.

Stewart, J.A., Weckhuysen, B.M. y Bruijnincx, P.C.A. (2015). Reusable Mg-Al hydrotalcites for the catalytic synthesis of diglycerol dicarbonate from diglycerol and dimethyl carbonate. *Catalysis Today 257*, 274-280.

Tanabe, K. (1970) Chapter 2 - determination of acidic properties on solid surfaces. En: *Solid Acids and Bases*, Pp. 5-33. Academic Press.

Xie, W., Peng, H., Chen, L. (2006). Calcined Mg-Al hydrotalcites as solid base catalysts for methanolysis of soybean oil. *Journal of Molecular Catalysis A: Chemical 246*, 24-32.

Yan, C., Xue, D. (2005). Novel self-assembled MgO nanosheet and its precursors. *The Journal of Physical Chemistry B, 2005 109*, 12358-12361.

Zarazúa-Aguilar, Y., Paredes- Carrera, S., Valenzuela-Zapata, M., Sánchez-Ochoa, J. . (2018). Cr (vi) and naftalene simultaneous degradation using layered double hydroxides CuZnGa. *Revista Mexicana de Ingeniería Química 12*, 679-691.

Zhang, L., Fu, W., Xiang, M., Wang, W., He, M., Tang, T. (2015). MgO nanosheet assemblies supported CoMo catalyst with high activity in hydrodesulfurization of dibenzothiophene. *Industrial & Engineering Chemistry Research 54*, 5580-5588.

Zhao, M.-Q., Zhang, Q., Huang, J.-Q., Tian, G.-L., Nie, J.-Q., Peng, H.-J., Wei, F. (2014). Unstacked double-layer templated graphene for high-rate lithium-sulphur batteries. *Nature Communications 5*, 3410, 1-8.

Zhao, R., Yin, C., Zhao, H. y Liu, C. (2003). Synthesis, characterization, and application of hydrotalcites in hydrodesulfurization of FCC gasoline. *Fuel Processing Technology 81*, 201-209.